PCCP

ROYAL SOCIETY OF CHEMISTRY

PAPER

View Article Online
View Journal | View Issue

Cite this: *Phys. Chem. Chem. Phys.*, 2025, **27**, 19170

Modulations in the binding selectivity of phenol and thiophenol with ethyl cinnamate: an IR spectroscopic and quantum chemical investigation

Puja Samanta and Pujarini Banerjee *

Complexes of (E)-ethylcinnamate (EC), a widely prevalent plant secondary metabolite, with two hydrogen bond donors phenol (Ph) and thiophenol (TPh), have been studied under ambient conditions in solution. The former, characterized by multiple electron-rich centers, offers multiple accessible sites to which the phenolic O–H donor or the thiophenolic S–H donor can bind. Experimental shifts in donor stretching frequencies as well as in signature vibrations of the acceptor EC molecule are interpreted in combination with quantum chemical calculations to assign the binding preferences of both Ph and TPh. It is observed that the phenolic O–H binds almost exclusively to the highly electronegative carbonyl oxygen on EC through an O–H···O H-bond. However, there is a loss of selectivity in the case of the thiophenolic S–H donor, which shows equal propensity to bind both to the oxygen centres through the S–H···O H-bond and to the more diffuse benzene π-cloud on EC, through the S–H···π H-bond. The observations suggest that the S–H···π H-bond is strong enough to compete with the S–H···O H-bond, unlike the O–H···π H-bond, which is always a weaker variant of the conventional O–H···O type. Noticeable changes are observed in predicted geometries at the H-bond interfaces for the thiophenolic complexes, as compared to the phenolic complexes. While dispersion plays a major role in the stabilization of both EC–Ph and EC–TPh complexes, the observed modulations in intermolecular binding are largely an outcome of the delicate interplay of electrostatic and dispersion interactions. Specific binding preferences appear to be the effect of inherent attributes of donor–acceptor groups. TPh, being an acid of "softer" nature, has a greater tendency to bind to the "softer" π-electron acceptor site on EC, compared to the "harder" phenolic donor Ph, which prefers the "harder" and more electronegative carbonyl oxygen site. The results lend additional insights into the subtle effects of heavier atom substitution on biomolecular recognition.

Received 29th May 2025,
Accepted 12th August 2025

DOI: 10.1039/d5cp02031j

rsc.li/pccp

1. Introduction

Sulphur-centered hydrogen bonds (H-bonds) have been considered to be of widespread importance in the past few decades. Although, in the initial understanding of H-bonds, sulphur was considered to be a poor participant owing to its lower electronegativity as compared to oxygen, nitrogen or halogens, there has been growing spectroscopic evidence of its role both as a H-bond donor and as a H-bond acceptor. The presence of sulphur in the side chains of two amino acids methionine and cysteine underlines its ubiquitous presence in proteins. Consequently, there has been growing interest in understanding various attributes of sulphur-centred non-covalent interactions, which are likely to contribute to protein secondary structures and molecular assemblies.[1–3] Some early reports involved the study of H_2S dimers in matrix isolation, where the shift of the S–H stretching frequency was attributed to H-bond formation.[4] In later years, extensive gas phase laser spectroscopic studies were carried out by Wategaonkar and co-workers to establish the potency of sulphur-centered H-bonds.[5] Red-shifts in the S–H stretching frequency were attributed to S–H···S H-bonding in the dimers of H_2S[6] and to S–H···O H-bonding in clusters of H_2S with methanol and various ethers.[7] The role of H_2S as a H-bond donor in S–H···π H-bonded complexes was detailed by Arunan *et al.* in their rotational spectroscopic studies of H_2S–benzene, where the H_2S donor was suggested to rotate freely above the plane of the benzene π-ring in a near-spherical potential.[8] Later the same complex was also characterized by gas phase electronic and infrared spectroscopy.[9] Evidence of S–H···π H-bonding was also obtained in LIF studies of H_2S–indole and H_2S–methylindole clusters.[10] An established aspect of H-bonds involving sulphur is the dominant contribution of dispersion interactions to overall binding stability, as compared to their counterparts involving oxygen or nitrogen.[1–3,5]

Department of Chemistry, Diamond Harbour Women's University, Sarisha, West Bengal, India. E-mail: pujarini.banerjee87@gmail.com

The participation of thiols in H-bonding has been shown in various studies over the past few decades. Early studies in the liquid phase indicated the presence of S–H···S H-bonding in thiophenols taken at concentrations of 1 M or higher in CCl_4.[11] The vibrational Stark effect on the S–H vibration in the S–H···π H-bonded complexes between thiophenol and a series of substituted benzenes was explored by Boxer and co-workers, and it was suggested that the electrostatic component is less important in the stabilization of such complexes, compared to their N–H···π and O–H···π counterparts.[12] Complexes of methanethiol with ammonia were studied using matrix isolation IR spectroscopy by Grzechnik *et al.*[13] Lobo *et al.* showed from their high resolution gas phase studies that the thiol group in 2-phenylethanethiol can act both as a H-bond donor and as a H-bond acceptor.[14] In a more recent microwave spectroscopic study, the competition between different sulphur centred H-bonds was studied for conformationally diverse pure and mixed dimers of 2-phenylethanethiol and 2-phenylethanol.[15] Also jet-cooled rotational spectroscopic studies of the thiophenol dimer showed that π-stacking interactions alongside S–H···S interactions were important in stabilizing the thiophenol dimer, as compared to the phenol dimer where stacking plays no major role.[16]

In the present work, a comparative study has been carried out in the liquid phase under thermal solvation in carbon tetrachloride between the H-bonded complexes of two different donors phenol (Ph) and thiophenol (TPh) with the same acceptor molecule (E)-ethyl cinnamate (EC). The phenolic O–H group is an important substituent in the side chain of the amino acid tyrosine, while the S–H group constitutes the side chain in cysteine. EC, on the other hand, is known for its acaricidal activity,[17] and is also an important plant secondary metabolite found in cinnamon and several other plant species.[18] The study of EC–Ph and EC–TPh complexes in solution may therefore have implications on the understanding of protein-mediated transfer of such metabolites across the cell membrane under ambient conditions.[19] In previous studies of sulphur-centred H-bonds, it has been shown that shifts in donor stretching frequencies as well as binding energies correlate with the proton affinity of the acceptor, for both S–H donor groups with oxygen containing acceptors and O–H donor groups with sulphur containing acceptors.[20,21] In such studies, the acceptor groups were constituted by localized lone pair orbitals on sulphur or oxygen. In the molecule EC of our present study, however, multiple electron-rich centers are available to act as acceptor sites for binding, like the lone pair electrons on the oxygen-containing groups, as well as the more diffuse π-electron density on the benzene ring, or on the C=C double bond in conjugation with it. The planarity of the EC molecule makes all such centers accessible to the approaching donor group. This gives rise to the possibility of an interplay between interactions of the type O–H···O and O–H···π for the phenolic donor, and analogous interactions of the S–H···O and S–H···π type for the thiophenolic donor. The objective of our work would be to determine whether binding preferences arising out of such interplay are modulated in the presence of the more polarizable and less electronegative sulphur-containing donor group on TPh, as compared to the oxygen donor group of Ph. The relationship of such binding preferences with the inherent attributes of the different acceptor sites is also to be explored. It has been stressed before that since the S–H stretching vibration is a spectral region that is free of other vibrations of common protein functional groups, it could be used as a probe to study sulphur-centred interactions in biological systems, despite its weaker oscillator strength.[12] Therefore, complexation-induced infrared shifts in the donor stretching fundamentals, υ_{O-H} and υ_{S-H}, and those in signature vibrations of the acceptor EC molecule, namely, $\upsilon_{C=O}$, υ_{C-O} and $\upsilon_{C=C}$ have been analyzed. The spectral observations are correlated with theoretical predictions of shifts and binding energies to determine binding preferences.

2. Materials and methods

Ethyl cinnamate was obtained from Merck, while phenol, thiophenol and the solvent CCl_4 were procured from Spectrochem India Pvt. Ltd. Phenol and thiophenol were distilled before use and checked for impurities. A homemade brass cell consisting of a pair of NaCl windows and Teflon spacers of thickness 0.1 mm was used for liquid phase sampling. The cell was placed in the chamber of a Bruker Alpha II FTIR spectrophotometer, which was equipped with a deuterated triglycine sulfate (DTGS) detector and a ZnSe beam-splitter. FTIR spectra were recorded at an instrumental resolution of 2 cm^{-1} over an average of 32 scans each, keeping in mind intrinsic band widths in the solution phase, while maximizing signal-to-noise ratios. In all cases, atmospheric compensation was duly carried out to account for the presence of water vapour.

Geometry optimizations were performed using the Gaussian 09 program package at the M06-2X/6-311++G(d,p) and ωB97XD/6-311++G(d,p) levels of theory,[22–25] in conjunction with the CPCM solvent model,[26] with CCl_4 as the chosen solvent dielectric. Zhao and Truhler's M06-2X functionals are known to predict reliable interaction energies for non-covalent interactions like H-bonding,[23,24] while ωB97XD is known to include empirical atom-atom dispersion corrections that are vital to non-bonded interactions.[25] Theoretical predictions using the former DFT functional are given in the main manuscript, while those using the latter are given in the SI. The vibrational frequencies for different conformations of EC and its complexes with Ph and TPh were computed at a harmonic approximation and checked to confirm minima on the potential energy surfaces. The scale factors for Ph and TPh were taken as 0.928 and 0.938, respectively, while that for EC was taken to be 0.951. Potential energy distributions of various normal modes of EC were ascertained using the VEDA 4.0 program.[27] Partitioning of the total binding energy of complexes into its various components was carried out using the GAMESS (US) program package, employing the localized molecular orbital (LMO) based energy decomposition analysis.[28] Bader's atoms in molecules (AIM) theory as implemented in the AIM2000 program package was also employed for analysis of the electron density topologies of the complexes.[29] Spectral peak

fittings were performed with Gaussian band profiles using the peak analyzer module of Origin Pro 8.5 software.

3. Results and discussion

3.1. Conformational distribution and IR spectrum of (*E*)-ethyl cinnamate

As predicted by CPCM solvent model calculations at the M06-2X/6-311++G(d,p) level of theory, EC exists as a number of conformers in CCl_4 solution, of which the lower energy ones are depicted in Fig. 1. The relative spatial orientations of the olefinic C2═C3 bond and the carbonyl C═O bond about the C1–C2 single bond gives rise to s-*cis* (EC-sc) and s-*trans* (EC-st) forms. Variations in the spatial orientation of the ethyl group give rise to additional conformers within both the s-*cis* and s-*trans* types. Considering all such predicted forms, the energy of the lowest energy conformer EC-sc1 is taken as 0.0 kcal mol^{-1}, and the energies of all other conformers are reported relative to it. It is observed that four such conformers lie within a narrow range of energies, and thus are likely to be appreciably populated under the thermal conditions of our experiment. The mid-infrared spectrum of 0.05 M EC is depicted in SI Fig. S1. Evidently the most intense band in EC at 1716 cm^{-1}, corresponds to the carbonyl stretch $\upsilon_{C=O}$, whereas the band to its red side at 1640 cm^{-1} corresponds to $\upsilon_{C2=C3}$, the olefinic C2═C3 stretching vibration. The bands centred at ~1175, 1202 and ~1310 cm^{-1} involve contributions from the C1–O stretching vibration. The PED analysis of relevant functional group vibrations and skeletal vibrations of EC corresponding to its most stable E-sc1 conformer is reported in Table T1, SI.

3.2. H-bonded complex of EC with phenol

3.2.1. Predictions of theory. The mapping of the electrostatic potential (ESP) surface of EC is shown in Fig. 2. It is evident that there are four distinct regions of negative electrostatic potential, to which a proton donor could bind, namely, the carbonyl oxygen (site 1), the ester oxygen (site 2), the benzene π-cloud (site 3), and the C2═C3 double bond in conjugation with it (site 4). As expected, the highest concentration of negative charge is observed at site 1 along the extension of the C═O bond (V_{max} = −0.054 a.u.) compared to lower values for sites 2 (V_{max} = −0.021 a.u.), 3 (V_{max} = −0.020 a.u.) and 4 (V_{max} = −0.016 a.u.). Therefore all initial input geometries for binary EC–Ph complexes were constructed considering the binding of the phenolic O–H donor to these four distinct regions of negative electrostatic potential.

The optimized geometries of the EC–Ph1, EC–Ph2 and EC–Ph3 complexes corresponding to binding at sites 1, 2 and 3, respectively, are depicted in Fig. 3. No complexes could be optimized corresponding to binding at site 4. All binding energies ($\Delta E_{b)}$ of complexes are obtained relative to the sum of the energies of the EC-sc1 and phenol monomers and include consideration for zero-point energies. Predictions at the M06-2X/6-311++G(d,p) level of theory suggest that there is a clear preference for complexes of types EC–Ph1 and EC–Ph2, as compared to EC–Ph3, as summarized in Table 1. The former two are bound by the conventional O–H···O H-bond while the latter involves the O–H···π H-bond. The presence of the H-bonds is confirmed by AIM analysis, where the electron densities at the corresponding bond critical points (BCP) are found to be of the range expected for such non-covalent interactions, as given in Table 2.[29,30] EC–Ph1 exists as two different conformers. In the former (EC–Ph1a), which is more stable (ΔE_b = 9.5 kcal mol^{-1}), the phenolic O–H approaches from the side of the benzene ring of EC, while in the latter (EC–Ph1b) the approach is from the side of the ethyl group of EC (ΔE_b = 7.4 kcal mol^{-1}). The former appears to drive its higher stability from the fact that the approach from the benzene ring-side of EC causes the two aromatic groups of either moiety to be partially stacked one above the other, leading to higher dispersion stabilization. The same is verified by energy decomposition analysis (EDA), where a

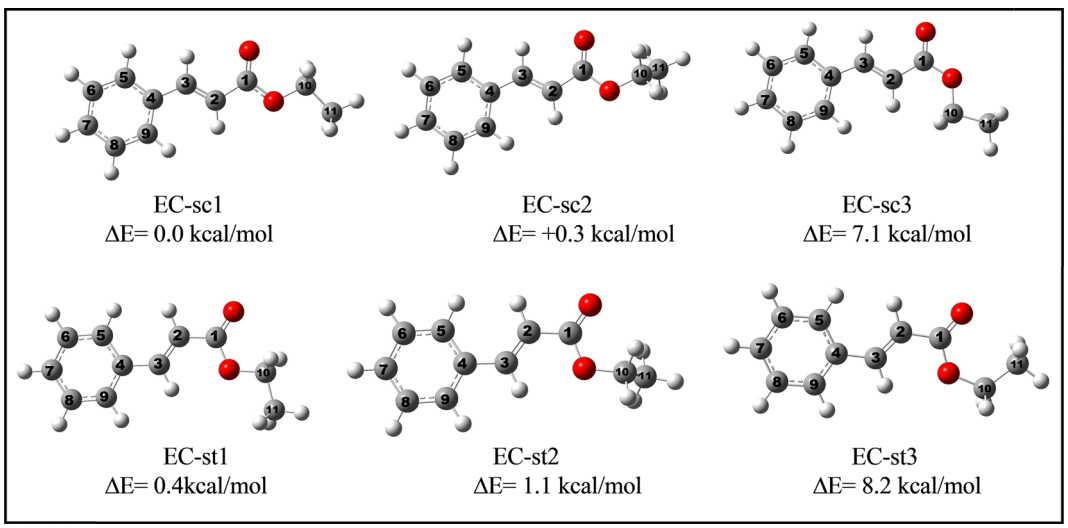

Fig. 1 Various conformers of EC predicted at the M06-2X/6-311++G(d,p) level of theory.

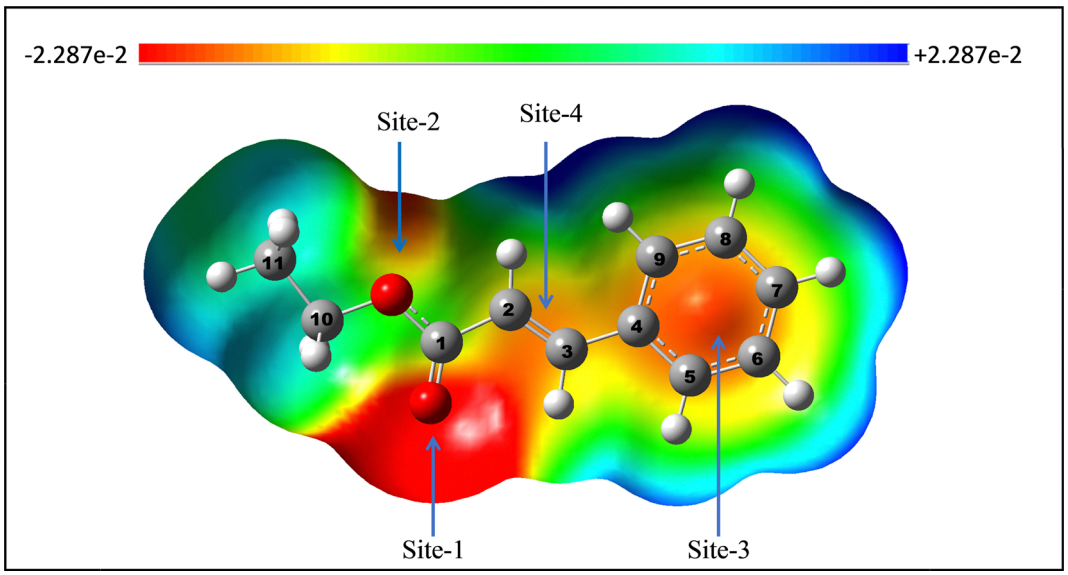

Fig. 2 ESP mapping of EC for the 0.0004 e Bohr^{-3} iso-density surface computed at the M06-2X/6-311++G(d,p) level of theory. Blue indicates positive potential while red indicates negative potential values.

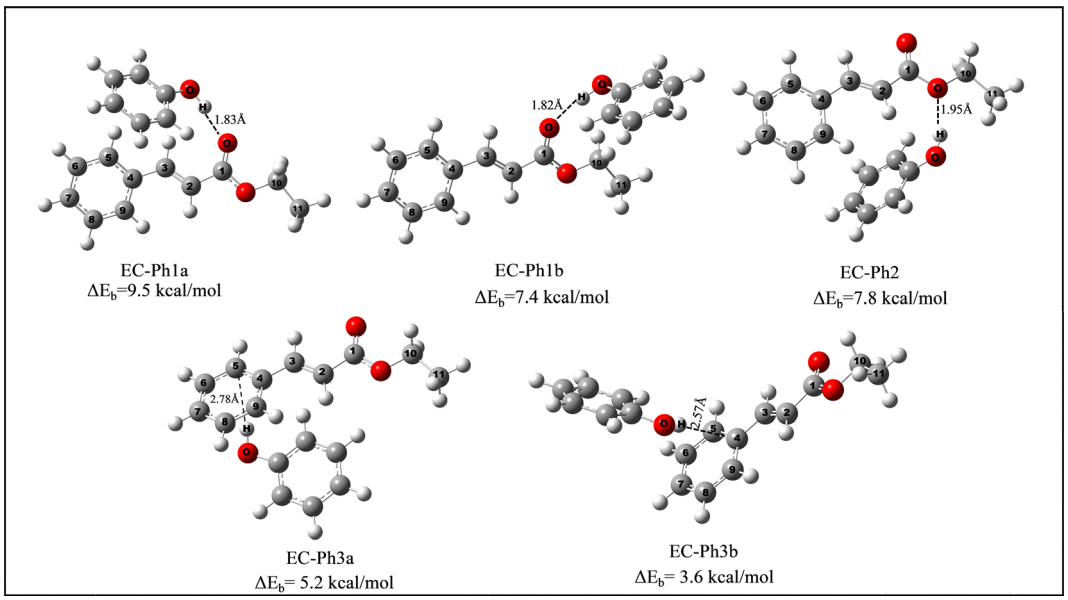

Fig. 3 Optimized geometries of EC–Ph complexes and their binding energies predicted at the M06-2X/6-311++g(d,p) level of theory.

higher contribution of the dispersion component is predicted for the former (−17.5 kcal mol^{-1}), compared to the latter (−10.8 kcal mol^{-1}), although the two complexes have similar electrostatic stabilization (Table 1). The binding energy for the ester–oxygen bound complex EC–Ph2 is predicted to be 7.8 kcal mol^{-1}, and also involves large dispersive stabilization (−18.9 kcal mol^{-1}). The involvement of the π-electrons as the acceptor site on EC also gives rise to two different conformations. In the more stable one EC–Ph3a (ΔE_b= 5.2 kcal mol^{-1}), phenol approaches from the direction of the C2═C3 double bond, such that the phenolic π-ring is nearly stacked parallel to the benzene π-ring on EC as well as to the C2═C3 double bond. The other conformer EC–Ph3b (ΔE_b = 3.6 kcal mol^{-1}) involves the approach of the phenolic ring from the benzene side of EC, resulting in a slanted T-shaped geometry at the H-bonded interface, with the phenolic O–H perched above one of the C═C double bonds in the benzene π-ring plane of EC (Fig. 3). This predicted geometry for EC–Ph3b is similar to many previous reports on π-H-bonded complexes involving O–H donors.[31,32] As observed from EDA, the higher stabilization for EC–Ph3a compared to EC–Ph3b is again due to the higher dispersive stabilization in the former (−15.7 kcal mol^{-1}), resulting from the π-stacked orientation, while the latter T-shaped conformer is less stabilized by dispersion (−9.2 kcal mol^{-1}), and also has a

Table 1 Energy decomposition analysis (EDA) depicting the partitioning of the total binding energy into its various components for various EC–Ph and EC–TPh complexes predicted at the M06-2X/6-311++G(d,p) level of theory

Conformer	Binding energy (kcal mol^{-1})	Electrostatic energy (kal mol^{-1})	Dispersion energy (kal mol^{-1})	Polarization energy (kcal mol^{-1})	Exchange energy (kcal mol^{-1})	Repulsion energy (kcal mol^{-1})
EC–Phenol						
EC–Ph1a	−9.5	−15.6	−17.5	−6.3	−12.4	39.3
EC–Ph1b	−7.4	−14.1	−10.8	−5.6	−9.6	30.0
EC–Ph2	−7.8	−11.9	−18.9	−3.9	−10.4	35.1
EC–Ph3a	−5.2	−5.8	−15.7	−1.5	−6.6	23.3
EC–Ph3b	−3.6	−3.4	−9.2	−1.5	−3.7	13.6
EC–Thiophenol						
EC–TPh1a	−7.1	−9.7	−17.3	−3.5	−9.5	31.1
EC–TPh1b	−1.1	−7.4	−13.6	−7.1	−2.3	23.9
EC–TPh2	−6.4	−8.0	−18.8	−2.3	−8.7	30.1
EC–TPh3a	−6.0	−6.4	−19.2	−1.5	−8.2	28.1
EC–TPh3b	−4.5	−4.9	−14.8	−1.3	−6.5	22.1

Table 2 Predictions of electron density topologies as well as spectral shifts of relevant vibrational modes for various EC–Ph and EC–TPh complexes

		$\Delta\nu_{O-H}$ (cm^{-1})		$\Delta\nu_{C=O}$ (cm^{-1})		$\Delta\nu_{C-O}$ (cm^{-1})	
Conformer	ρ_{BCP} O–H···O/π (a.u.)	Expt.	Theory	Expt.	Theory	Expt.	Theory
EC–Ph1a	0.0288	−192	−232.0	−18	−40.2	−19	+11.5
EC–Ph1b	0.0298		−221.5		−32.9		+10.3
EC–Ph2	0.0234		−134.0		+16.0		−25.3
EC–Ph3a	0.0064		−47.6		+0.8		−0.1
EC–Ph3b	0.0088		−47.6		+3.2		+1.8
		$\Delta\nu_{S-H}$ (cm^{-1})		$\Delta\nu_{C=O}$ (cm^{-1})		$\Delta\nu_{C2=C3}$ (cm^{-1})	
	ρ_{BCP} S–H···O/π (a.u.)	Expt.	Theory	Expt.	Theory	Expt.	Theory
EC–TPh1a	0.0155	−22	−59.3	−1.5 and −11	−24.1	−4	−13.8
EC–TPh1b	0.0132		−61.4		−3.2		+0.7
EC–TPh2	0.0134		−27.9		+5.1		−6.9
EC–TPh3a	0.0068		−33.1		−0.7		−6.8
EC–TPh3b	0.0071		−37.6		+0.6		−5.8

$\sim$2.4 kcal mol^{-1} lower contribution from electrostatics (Table 1). Similar geometries and binding energies are predicted using the ωB97XD method at the same level of calculation, as summarized in Table T2, SI.

3.2.2. IR spectra of the EC–Ph mixture

3.2.2.1. υ_{O-H} region. The traces a(black) and b(red) of Fig. 4 depict the spectra of pure 0.02 M Ph and 0.15 M EC in CCl_4, respectively, while the upper traces c to g depict the spectra of mixtures of EC and Ph for which the concentration of Ph is kept constant at 0.02 M, and the Ph to EC molar ratios are varied from 1 : 2.5 to 1 : 7.5. The concentration of Ph is so taken so as to minimize self-dimerization by H-bonding, and this is confirmed by the absence of any distinct bands to the red-side of the monomeric υ_{O-H} band at $\sim$3611 cm^{-1} for pure Ph [trace-a (black), Part A, Fig. 4]. However, in the presence of EC, a prominent broad feature centered at 3419 cm^{-1} appears. This red-shifted band in the phenolic υ_{O-H} region is attributed to formation of the binary complex between EC and Ph. Table 2 summarizes the experimental and predicted shifts for the complexes of the present study. The observed red shift of $\sim$192 cm^{-1} is comparable with the predicted red-shifts of 232.0 and 221.5 cm^{-1} for the EC–Ph1a and EC–Ph1b complexes, respectively. A closer observation of the νO–H band profile also reveals an asymmetry on the blue side of the band centre at 3419 cm^{-1}, suggesting other overlapped band components. The broad hump at $\sim$3475 cm^{-1} may be indicative of the complex EC–Ph2, since its shift of −136 cm^{-1} from the monomer is close to the υ_{O-H} shift of −134.0 cm^{-1} predicted for this complex. The predicted υ_{O-H} shift for the complexes EC–Ph3a and EC–Ph3b is −47.6 cm^{-1}, but no bands in this range are discernible. In previous studies of π-hydrogen bonded phenol complexes in solution by Zheng *et al.*, a high relative concentration of the π-acceptor molecule was necessary to decipher signatures of π–H-bonding in the υ_{O-H} region.[33] We therefore acquired additional data for this spectral region for higher concentrations of the acceptor EC molecule in CCl_4, while maintaining the same Ph concentration of 0.02 M. Further, thin films of Ph–EC mixtures were also prepared, with Ph/EC/CCl_4 in molar ratios of 1 : 10 : 50, similar to the concentrations used by Zheng *et al.* for phenol–benzene complexes.[33] However, no additional bands were observed corresponding to O–H···π interaction, suggesting that the lower binding energy of EC–Ph3 compared to that of EC–Ph1 leads to the latter's absence even under thermal solvation conditions.

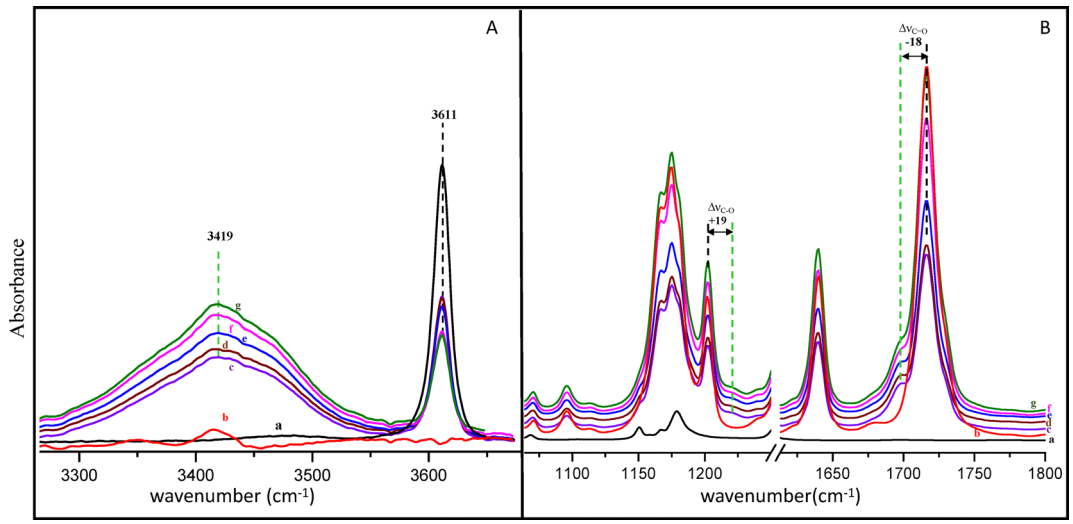

Fig. 4 IR spectra in the υ_{O-H} region of phenol (Ph, Part A) and the $\upsilon_{C=O}$ and υ_{C-O} regions of EC (Part B) depicting new spectral features upon EC–Ph complex formation (shown in light green vertical dashed lines) relative to corresponding monomer bands (black vertical dashed lines). The traces a (black) and b (red) depict pure 0.02 M Ph and 0. 15 M EC in CCl_4, respectively, while the upper traces c–g depict the spectra of mixtures of 0.02 M Ph with varying EC concentrations. Traces c–g represent 1 : 2.5, 1 : 3.5, 1 : 5, 1 : 6.5, and 1 : 7.5 Ph to EC molar ratios in CCl_4, respectively.

3.2.2.2. $\upsilon_{C=O}$ and υ_{C-O} regions. Another noticeable effect of complex formation is observed corresponding to the $\upsilon_{C=O}$ transition of EC. While the monomer band appears at ~1716 cm^{-1}, a distinct shoulder arises at ~1698 cm^{-1}, *i.e.*, at a red shift of 18 cm^{-1} (traces c–g, Part B, Fig. 4). The intensity of this band is found to increase with increasing concentration of EC and is therefore attributed to the EC–Ph binary complex. Our theoretical calculations for the EC–Ph1a, EC–Ph1b, EC–Ph2, EC–Ph3a and EC–Ph3b complexes predict $\upsilon_{C=O}$ shifts of −40.2, −32.9, +16.0, +0.8 and +3.2 cm^{-1}, respectively, suggesting that the spectral observations are most consistent with the formation of the EC–Ph1 type of complex. Since no blue shifted bands are formed in this region, the presence of the EC–Ph2 complex, despite its comparable binding energy with EC–Ph1, appears to be ambiguous, and one reason could be the involvement of the lone pair electrons on the ester oxygen in a conjugative interaction with the carbonyl group. This suggestion is further substantiated from observations in the region of the υ_{C1-O} vibration. A new band, whose intensity is again found to increase with increasing concentration of EC in the EC–Ph mixture (Fig. 4B), is observed at ~1221 cm^{-1}. This band develops as a shoulder of the band at ~1202 cm^{-1}, which is assigned to the C1–O stretching vibration. In agreement with this experimental shift of +19 cm^{-1}, blue shift of this vibration is predicted by theory for the EC–Ph1a

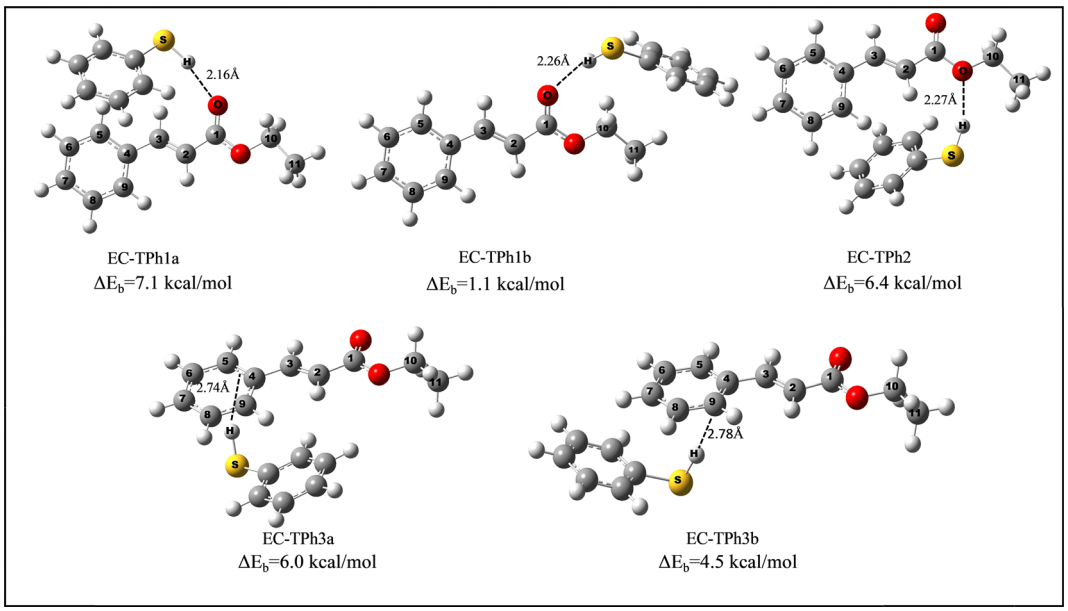

Fig. 5 Optimized geometries of EC–TPh complexes and their binding energies predicted at the M06-2X/6-311++g(d,p) level of theory.

(+11.5 cm^{-1}) and EC–Ph1b (+10.2 cm^{-1}) complexes, respectively. On the other hand, a red shift of the same vibration (−25.3 cm^{-1}) is predicted for the EC–Ph2 complex, while the shifts predicted for complexes EC–Ph3a and EC–Ph3b are −0.1 and +1.8 cm^{-1}, respectively. Overall, the observed shifts for the υ_{O-H} band of the H-bond donor Ph and those for the $\upsilon_{C=O}$ and υ_{C1-O} bands of the H-bond acceptor EC lead us to infer that under thermal conditions the EC–Ph1 complex is almost exclusively formed, although the possible presence of EC–Ph2 may not be ruled out altogether considering the observations in the νO–H region, and its comparable binding energy with the former. This is confirmed further from calculations at the ωB97XD/6-311++G(d,p) level of theory, which predict similarly, as shown in Table T2, SI.

3.3. H-bonded complexes of EC with thiophenol

3.3.1. Predictions of theory. Our search for stable complexes of thiophenol with the same proton acceptor EC (EC–TPh) led us to choose the same starting geometries as those obtained for the optimized EC–Ph complexes, with only the S–H donor replacing the phenolic O–H donor. The various geometries optimized for the three different kinds of complexes, EC–TPh1, EC–TPh2 and EC–TPh3, are shown in Fig. 5 below, corresponding to the binding of TPh to electron rich sites 1, 2 and 3 of EC, respectively. Similar to the EC–Ph complexes, no geometries corresponding to binding at site 4 could be optimized. Despite the apparent similarity of binding in EC–Ph and EC–TPh complexes, a few remarkable differences are observed for the latter. EC–TPh1 optimizes in two conformations, EC–TPh1a and EC–TPh1b, involving a S–H···O H-bond. In the former, the TPh moiety approaches the carbonyl group of EC from the side of the latter's benzene ring, such that the π-ring plane of TPh is in a displaced π-stacked orientation with respect to that of EC. On the other hand, the latter geometry involves the approach of the thiophenolic S–H group from the direction of the ethyl group of EC, whose benzene π-ring remains perpendicular to the π-ring of TPh, and away from it. Unlike the EC–Ph1 complexes, the donor S–H bond does not remain in the same plane as the thiophenolic π-plane, as is evident from Fig. 5. While the S–H bond in EC–TPh1a is only slightly displaced with respect to the π-plane (H–S–C–C dihedral = 12.824°), that in EC–TPh1b is largely displaced from the π-plane (H–S–C–C dihedral = 50.925°). EC–TPh1a is predicted to have a ΔE_b of 7.1 kcal mol^{-1}, which is much higher than that of EC–TPh1b (ΔE_b = 1.1 kcal mol^{-1}). This suggests that the π-stacking interaction plays a more vital role in the stabilization of the S–H···O hydrogen bond, as compared to the O–H···O H-bond in analogous complexes of EC and Ph, where the difference in ΔE_b values between EC–Ph1a (ΔE_b = 9.5 kcal mol^{-1}) and ECPh1b (ΔE_b =7.4 kcal mol^{-1}) is much lower (Section 3.2.1). In the jet-cooled microwave studies of the thiophenol dimer by Saragi *et al.*,[16] the influence of such dispersion-controlled π-stacking, alongside S–H···S H-bonding, on the geometry of the dimer was analyzed in comparison with that of the O–H···O H-bonded phenol dimer, where dispersion has a lower effect. In our case, the benzene π-ring of EC evidently modulates the binding interface of the EC–TPh1 complexes to a large extent, leading to a preference for the π-stacked complex EC–TPh1a.

The optimized complexes of TPh with binding sites 2 and 3 are also depicted in Fig. 5. The structure of EC–TPh2 is analogous to that of EC–Ph2, while the π-bound complex, similar to the case of phenol, optimizes in two conformations, the more stable one (EC–TPh3a) involving the approach of the thiophenolic group from the side of the C2=C3 bond, leading to π-stacked orientation, and the latter (EC–TPh3b) involving the approach of thiophenol from the side of the benzene ring of EC. The binding energies of TPh2 and TPh3a are predicted to be 6.4 and 6.0 kcal mol^{-1}, respectively, which are quite comparable to that of TPh1a (ΔE_b =7.1 kcal mol^{-1}) and much higher than that of TPh1b. Unlike for EC–Ph, where there is a clear preference for the O–H···O H-bonded conformers, the comparable energies of binding of TPh to all the three sites means that upon substitution of the O–H donor in phenol by its heavier analogue S–H, there is a loss of selectivity in binding. Under the conditions of thermal solvation, the S–H donor has a comparable propensity to dock on any of the multiple electronegative sites on the acceptor EC molecule. A closer look at the optimized geometries reveals a most striking difference in the H-bonded interface of both conformers of EC–TPh3 compared with the analogous π–H-bonded conformers of EC–Ph3. At the given level of theory, the S–H bond in EC–TPh3a is predicted to be twisted completely out of planarity with the thiophenolic π-ring, giving a value of 66.541° for the H–S–C–C dihedral, while for the analogous phenolic complex EC–Ph3a, the O–H bond remains much more co-planar with the phenolic π-ring ($\delta_{H-O-C-C}$ = 17.0°). The difference between the complexes EC–TPh3b and EC–Ph3b is also rather pronounced, since for the former, the approach of thiophenol from the benzene side of EC causes the thiophenolic ring to orient in a distorted π-stacked orientation with the benzene ring, while the S–H bond twists completely out of planarity ($\delta_{H-S-C-C}$ = 99. 275°) to point towards the π-cloud. The phenolic O–H bond in EC–Ph3b, on the other hand, remains in the plane of the aromatic ring. A slight distortion of the S–H bond from planarity (by 15.772°) is also predicted for EC–TPh2, unlike the analogous complex EC–Ph2, where the O–H bond remains co-planar with the Ph π-ring, as in the monomer.

3.3.2. IR spectra of the EC–TPh mixture. As mentioned in previous liquid phase studies of TPh, the tendency of the S–H donor to engage in H-bonding is observable at comparatively higher molar concentrations than the O–H donor.[11,12] The weaker polarity of the S–H bond compared to the O–H bond, as well as the former's larger inter-nuclear separation, may be the reason for such manifestation. In our experiments, concentrations of both TPh and EC have been optimized to understand IR spectral effects of complex formation in different regions. Part A of Fig. 6 depicts changes in the υ_{S-H} region of the TPh donor upon complex formation, while part B depicts changes in the $\upsilon_{C=O}$ and $\upsilon_{C2=C3}$ regions of the acceptor EC.

3.3.2.1. υ_{S-H} region. The spectra of pure TPh and pure EC in CCl_4 are shown in traces a and b, respectively, while the difference spectra corresponding to formation of the complex between 0.2 M TPh and varying concentrations of EC are depicted in traces c–g, after necessary subtraction of contributions from the same concentrations of the pure components.

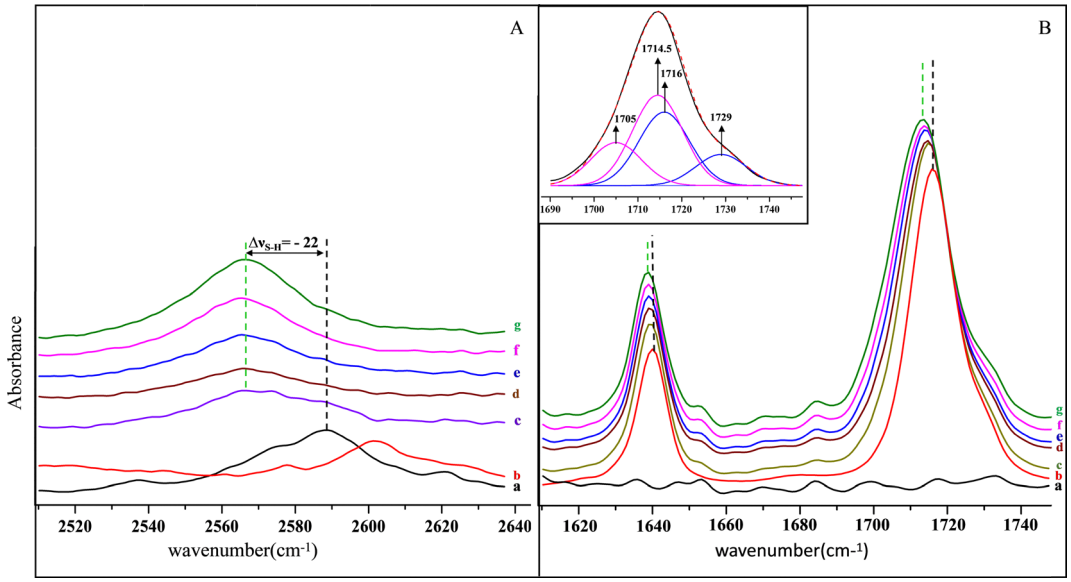

Fig. 6 IR spectra in the υ_{S-H} region of thiophenol (TPh, Part A) and the $\upsilon_{C=O}$ and $\upsilon_{C2=C3}$ regions of EC (Part B) depicting new spectral features upon EC–TPh complex formation (shown in light green vertical dashed lines) relative to corresponding monomer bands (black vertical dashed lines). The traces a (black) and b (red) in Part A depict pure 0.2 M TPh and 0.2 M EC in CCl_4, respectively, while the upper traces c–g depict the difference spectra of mixtures of 0.2 M TPh with varying EC concentrations. Traces c–g represent 1 : 0.25, 1 : 0.35, 1 : 0.5, 1 : 0.75 and 1 : 1 TPh to EC molar ratios in CCl_4, respectively. Part B depicts spectral changes when 0.1 M EC is complexed in molar ratios of 1 : 10 (trace c), 1 : 15 (trace d), 1 : 20 (trace e), 1 : 25 (trace f) and 1 : 30 (trace g) with TPh, respectively. Traces a and b in Part B depict pure TPh (1.5 M) and EC (0.1 M) in CCl_4. The inset depicts a curve fitting in the $\upsilon_{C=O}$ region for the 1 : 15 EC to TPh molar ratio, showing two new bands (pink colour) at ~1714.5 and ~1705 cm^{-1} due to complex formation, i.e., at shifts of −1.5 and −11 cm^{-1} from the primary monomer band (blue) at ~1716 cm^{-1}.

The original spectra without any subtractions are given in SI Fig. S2. It is observed from Fig. 6A that a new band, centred at ~2566 cm^{-1}, *i.e.*, at a red shift of ~22 cm^{-1} from the monomeric S–H stretching vibration, is formed as a result of complex formation. (As shown in SI Fig. S3, in the concentration variation spectra of TPh itself, the monomer band appears at ~2588 cm^{-1}, while the self-dimer band appears at ~2572 cm^{-1}. At the concentration of 0.2 M TPh taken for this set, both monomer and dimer contributions are subtracted to give the difference spectra c–g attributed only to complex formation.) The predicted υ_{S-H} shifts for formation of the S–H···O H-bonded complexes EC–TPh1a and EC–TPh2 are −59.3 and −27.9 cm^{-1}, respectively, while that of the S–H···π H-bonded complexes of EC–TPh3a and EC–TPh3b are −33.1 and −37.6 cm^{-1}, respectively. Judging by this spectral region, there is possibility for formation of all of the above complexes EC–TPh1, EC–TPh2 and EC–TPh3, including the π-bound complex, since the magnitude of the observed υ_{S-H} shift is of the same range as that reported previously for S–H···π H-bonded complexes in solution.[12] Another noticeable feature of complex formation in the υ_{S-H} spectral region is the large enhancement in intensity of the υ_{S-H} vibration as compared to the uncomplexed form. The same was reported previously in the liquid phase as well as matrix isolation studies of complexes involving thiol donors[12,13] and attributed to the large polarizability of the S–H bond, as well the behaviour of its dipole moment function.

3.3.2.2. $\upsilon_{C=O}$ and $\upsilon_{C=C}$ regions. As in the case of the EC–Ph complex, the $\upsilon_{C=O}$ band of EC undergoes changes upon complex formation with TPh, as shown in Fig. 6B. Spectra have been obtained for 0.1 M EC in CCl_4 for varying molar ratios with TPh, ranging from 1 : 10 to 1 : 30. It is observed that the effects of H-bond formation in solution for the thiophenolic donor are more subtle than those for the phenolic donor. In the concentration range taken, the $\upsilon_{C=O}$ band centre shifts between 1 and ~4 cm^{-1} to the red-side, the higher shift for higher TPh concentration in the mixture. The curve-fitted spectrum for the mixture of EC and ThPh taken in the ratio of 1 : 15 is shown in the inset of Part B, Fig. 6. The fitting reveals two underlying components at ~1714.5 and ~1705 cm^{-1} in addition to the monomer band at ~1716 cm^{-1}, suggesting formation of more than one kind of complex. Considering the absence of a clear isosbestic point, and the possible self-association of TPh for the concentrations taken, it cannot be said with certainty that the complexes are in a 1 : 1 stoichiometric ratio, although steric considerations lead us to assume that the solution is dominated by binary, rather than higher complexes. The possible spectral effect of ternary (or higher association) has been considered in electronic structure calculations, as discussed later in the same section.

Regarding the predictions for the EC–TPh binary complexes, the $\upsilon_{C=O}$ shifts are predicted to be −24.1, +5.1 and −0.7 cm^{-1} for EC–TPh1a, EC–TPh2 and EC–TPh3a, respectively. The shift of this vibration may be attributed to its direct involvement as a H-bonding site (as for the former), and/or to energy redistribution of the normal mode upon complex formation. As discussed in the previous section, energetic considerations predict a comparable propensity for binding of TPh to all three sites. However, the absence of any blue-shifted band in this spectral

region leads us to infer that the binding through site 2 is improbable, although it cannot be ruled out altogether considering the υ_{S-H} region. The band positions of the fitted components within the $\upsilon_{C=O}$ band profile at $\sim$1714.5 cm^{-1} and 1705 cm^{-1} *i.e.*, at shifts of $\sim$1.5 and $\sim$11 cm^{-1} respectively, from the monomer, are a reasonable match with the predicted $\upsilon_{C=O}$ band positions for EC–TPh3a ($\Delta\upsilon_{C=O}$ = −0.7 cm^{-1}), and EC–TPh1a ($\Delta\upsilon_{C=O}$ = −24.1 cm^{-1}), respectively. Additional effects of EC–TPh complex formation involve the olefinic $\upsilon_{C2=C3}$ vibration of the acceptor EC. It is observed that the monomer band centre at 1640 cm^{-1} shifts to the red side by 0.5 to 1 cm^{-1}, as the concentration of TPh is increased (Fig. 6B and Fig. S4, SI). A curve fitting of the band profile reveals a component at $\sim$1636 cm^{-1} in addition to the monomer component, which is attributed to the EC–TPh complex (Fig. S4). The predicted shifts for this vibration are −13.8, −6.9, −6.8 and −5.8 cm^{-1} for EC–TPh1a, EC–TPh2, EC–TPh3a, and EC–TPh3b, respectively, which are comparable to the observed red shift of $\sim$4 cm^{-1}. Overall, the observed spectral changes indicate the co-existence of both S–H$\cdots\pi$ and S–H$\cdots$O (carbonyl oxygen bound and ester oxygen bound) interactions in the EC–TPh complex under thermal solvation.

The effect of higher association is taken into consideration theoretically by optimizing ternary complexes consisting of one molecule of EC and two molecules of TPh, since the latter is likely to self-associate through S–H$\cdots$S H-bonding at the concentrations taken. Calculations have been carried out for such 1 : 2 complexes using a more moderate basis set 6-31G(d,p). In the optimized trimers (SI, Fig. S5), the binding of the TPh dimer (TPh-d) to EC receptor sites 1 and 3 (EC–TPh-d-1 and EC–TPh-d-3) has been considered. The predicted $\upsilon_{C=O}$ shifts for these 1 : 2 complexes (unscaled) are −47.9 and −3.7 cm^{-1}, respectively, which are higher than those predicted at the same level of theory for the 1 : 1 complexes of EC–TPh1a (−34.1 cm^{-1}) and EC–TPh3 (−1.6 cm^{-1}), respectively. This means that the formation of higher complexes induces higher red-shifts of the $\upsilon_{C=O}$ transition, as also observed in solution for increasing concentrations of TPh in the mixture. It may also be stated that the S–H$\cdots\pi$ H-bonded ternary complex EC–TPh-d-3 is predicted to be 3.3 kcal mol^{-1} more stable than the corresponding ternary S–H$\cdots$O H-bonded ternary EC–TPh-d-1 complex. This implies that at higher concentrations of TPh in the EC–TPh mixture, the S–H$\cdots\pi$ interaction is more preferred.

3.4 Selectivity in binding: phenol *vs.* thiophenol

3.4.1. Interplay of electrostatic and dispersive interactions. The above observation that the complex EC–TPh exists both as S–H$\cdots$O and S–H$\cdots\pi$ H-bonded conformers, while the EC–Ph complex exists exclusively prefers the O–H$\cdots$O H-bonded interaction, suggests a marked difference in binding selectivity when sulphur, the heavier analogue of oxygen, participates in H-bonding. Clearly the phenolic O–H donor prefers the more electronegative acceptor site (V_{max} = −0.054 a.u.) consisting of the localized lone pair electrons on the carbonyl oxygen, while the thiophenolic donor shows an equal propensity for binding to this site as well as the less electronegative and more diffuse π-acceptor site on the benzene ring of EC (V_{max} = −0.020 a.u.). The primary difference in the nature of the two chemically analogous donors is the electronegativity of the chalcogen atom involved. The sulphur atom weakens the S–H dipole considerably, but its larger size also makes it more polarizable. The exclusive preference of the phenolic O–H to bind to the oxygen acceptor seems to be primarily driven by the electrostatic factor. As observed from the EDA (Table 1) of the complexes EC–Ph1a and EC–Ph3a (the more stable conformers of the carbonyl bound and π-bound complexes, respectively), the dispersion contributions are similar (−17.5 and −15.7 kcal mol^{-1}, respectively), while the electrostatic contribution for the former (−15.6 kcal mol^{-1}) is much higher than that of the latter (−5.8 kcal mol^{-1}). As discussed before, the large contribution of the dispersion component to overall binding energy for both the above complexes is an outcome of the π-stacking interactions between the phenolic π-cloud and the benzene π-cloud on EC. Also, the EDA results for EC–Ph3a are consistent with previous observations that unlike conventional H-bonds, weaker variants of type O–H$\cdots\pi$ are stabilized primarily by dispersion.[12,31] Between the multiple acceptor sites on EC however, the strong phenolic O–H dipole clearly favours the electrostatic interaction with the polar carbonyl group rather than with the diffuse π-cloud of benzene, *i.e.*, dispersion contributions being similar, electrostatics plays the decisive role in binding preferences. This leads to a considerably higher binding energy (ΔE_b= 9.5 kcal mol^{-1}) for the carbonyl bound complex, compared to that of the π-bound complex (ΔE_b= 5.2 kcal mol^{-1}), leading to the former's dominance even under thermal solvation conditions. Also, larger magnitudes of polarization stabilization are predicted for the carbonyl bound, rather than the π-bound complexes (Table 1). The EC–Ph2 complex (ΔE_b = 7.8 kcal mol^{-1}), though poorly evidenced in solution, also has higher magnitudes of electrostatic, dispersion and polarization stabilization than the π-bound complex.

The domination of dispersion to overall stability is more pronounced for complexes involving the S–H donor, whether carbonyl bound or π-bound. For example, the contribution of electrostatic interactions for the carbonyl bound complex EC–TPh1a is −9.7 kcal mol^{-1}, while that of dispersion is −17.3 kcal mol^{-1}. As stated in the Introduction, many existing studies have suggested that dispersion interactions indeed dominate over electrostatic interactions for H-bonds involving sulphur. Evidently, S–H being the weaker dipole, electrostatic interactions are subdued compared to the O–H donor in phenol. So for the analogous carbonyl-bound complexes EC–Ph1a and EC–TPh1a, the dispersion stabilization has very similar values (−17.5 and −17.3 kcal mol^{-1}, respectively), while the electrostatic stabilization is $\sim$6 kcal mol^{-1} lower in the thiophenolic complex, leading to a lower value of the resultant binding energy for the latter (ΔE_b = 7.1 kcal mol^{-1}) than the former (ΔE_b = 9.5 kcal mol^{-1}). However, the interplay between electrostatic and dispersion interactions is more subtle for complexes with the thiophenolic donor. EDA shows that for the π-bound EC–TPh3a complex, the electrostatic contribution is somewhat lower (−6.4 kcal mol^{-1}), but not markedly lower,

than that of the carbonyl-bound EC–TPh1a (−9.7 kcal mol^{-1}), while the dispersion contribution for the former is somewhat higher (−19.2 kcal mol^{-1}) than that of the latter (−17.3 kcal mol^{-1}). The different contributions to the binding energy of EC–TPh2 are also similar (Table 1). Other component interactions being comparable, all complexes have comparable binding energies, leading to a loss of binding selectivity for the S–H donor. This also means that the same π-acceptor site on EC has a higher binding affinity for the thiophenolic S–H donor, compared to the phenolic O–H donor. Indeed, the binding energy of the π-bound thiophenolic complex EC–TPh3a (ΔE_b= 6.0 kcal mol^{-1}) is predicted to be higher than that of the analogous phenolic complex EC–Ph3a (ΔE_b= 5.2 kcal mol^{-1}), contrary to the trend observed for the carbonyl-bound complexes EC–TPh1a and EC–Ph1a. Energy partitioning reveals that although the contributions of the electrostatic component are similar for EC–Ph3a and EC–TPh3a (−5.8 and −6.4 kcal mol^{-1}, respectively), that of dispersion is higher for the latter (−19.2 kcal mol^{-1}) than that for the former (−15.7 kcal mol^{-1}). It may also be noted that the contributions of the polarization components are predicted to be the same for both (−1.5 kcal mol^{-1}). Our findings bear resonance with previous suggestions from gas-phase studies of H_2S–indole clusters by the group of Wategaonkar that the S–H$\cdots\pi$ interaction is indeed stronger than the O–H$\cdots\pi$ interaction.[10] Evidently, it is the delicate balance of the underlying electrostatic, dispersion and other interactions not just at the H-bonded interface but between each pair of atoms in the molecular complex that manifests in such subtle modulations in binding preferences.

3.4.2. Effect on intermolecular geometry. The above observation that stabilities of the EC–Ph and EC–TPh complexes are driven by a delicate balance of electrostatic and dispersion interactions manifests noticeably in the geometries at their H-bonded interfaces, and it can be seen that the phenolic/thiophenolic π-ring as well as the benzene π-ring of EC play important roles in geometry preferences. As stated above in Section 3.3.1, in the π-bound thiophenolic complexes EC–TPh3a and EC–TPh3b, the S–H bond twists out of the plane of the thiophenolic π-ring, which orients in a π-stacked orientation with respect to the benzene π-ring of EC, leading to large dispersive stabilization (Fig. 5). On the other hand, for the more stable π–H-bound phenolic complex EC–Ph3a, although the phenolic ring is π-stacked with the benzene π-ring of EC, the O–H donor remains co-planar with the former. In the less stable π-bound conformer EC–Ph3b, such π-stacking is absent, resulting in a slanted T-shaped structure (Fig. 3).

3.4.3. Relation with hardness/softness of donor–acceptor. In our study, the H-bond acceptor molecule EC contains multiple acceptor sites, consisting of both lone pair electrons and π-electrons, which compete for the O–H/S–H donor. It is evident that in terms of electronegativity (given by V_{max} values on ESP mapping), the former is a more potent H-bond acceptor group than the latter. Clearly the more polar phenolic O–H donor is guided by the higher electronegativity of the carbonyl site, leading to high electrostatic stabilization, while π–H-bonding remains energetically disfavoured. However, the propensity of the less polar thiophenolic S–H donor to equally prefer the π-acceptor group alongside the carbonyl acceptor group appears to conform with the ''soft'' nature of both the S–H donor and π-acceptor moieties. It is known that the difference in energies of the HOMO and LUMO orbitals of a molecule is a measure of its hardness or softness, a higher value indicating ''harder'' nature and *vice versa*. In the molecule EC, the lone-pair orbital on the carbonyl oxygen is a ''harder'' site than the π-acceptor site. As a quantitative measure of hardness/softness, the HOMO–LUMO energy gap ($\Delta E_{HOMO-LUMO}$) has been calculated separately for two prototype acceptor fragments of EC, namely formaldehyde, containing the carbonyl acceptor group, and benzene, the π-acceptor group. The value for the former is 9.18 eV while that for the latter is 8.42 eV, indicating that the benzene π-acceptor is the softer of the two centres, and therefore is more likely to prefer the softer S–H donor ($\Delta E_{HOMO-LUMO}$=7.47 eV) than the harder O–H donor ($\Delta E_{HOMO-LUMO}$ = 7.77 eV). It may be inferred therefore that H-bonding involving the thiophenolic sulphur atom as the donor is not only dependent on the electronegativity of the acceptor group, but also on the latter's hardness/softness. It is the balance of these two different factors that guides its binding preferences. In this case, the formation of the S–H$\cdots$O H-bonded EC–TPh1a complex is driven by the electronegativity of the carbonyl oxygen on EC, while the EC–TPh3 complex derives similar stability from the favourable interaction between the soft S–H donor group of TPh and the soft π-acceptor group on EC. These binding preferences are rather distinct from those of the analogous phenolic O–H donor, which is harder by nature, and therefore always prefers the harder carbonyl site with higher electronegativity.

4. Summary and conclusion

The study of H-bonded complexes of ethyl cinnamate with H-bond donors phenol and thiophenol reveals the possibility of multiple binding sites, corresponding to multiple regions of negative electrostatic potential on the former. In both cases, stable conformers are predicted, corresponding to binding at the carbonyl oxygen site, the ester oxygen site and the benzene π-cloud on EC. For the phenol donor, O–H$\cdots$O H-bonding to the oxygen sites is predicted to be much more favourable than O–H$\cdots\pi$ H-bonding to the benzene site. On the other hand, comparable energies of binding to all three sites are predicted for the thiophenol donor. IR spectroscopic observations under ambient conditions reveal an almost exclusive preference of the phenolic O–H donor for the carbonyl oxygen site on EC, and an even preference of the thiophenolic S–H donor for both the carbonyl oxygen and the benzene π-cloud. For both EC–Ph and EC–TPh complexes, experimental evidence of binding to the ester oxygen site is ambiguous, possibly because of the engagement of its lone pair electrons in a conjugative interaction with the carbonyl group. There is therefore a loss of binding selectivity in the case of the sulphur-centred H-bonded interactions with EC, as compared to oxygen-centred ones. Such modulations in binding preferences appear to owe their origin to subtle variations in the interplay of electrostatic and

dispersion interactions. As a result, distinct differences are observed in predicted intermolecular geometry for the EC–TPh complexes, as compared to EC–Ph complexes. The specific affinity of the phenolic or thiophenolic donor for a particular binding site on EC appears to be an outcome of the balance between polarity/electronegativity and the hardness/softness of the donor–acceptor sites. Phenol being the more polar and "harder" H-bond donor prefers the more electronegative and "harder" acceptor site on the carbonyl oxygen, while thiophenol being less polar and "softer" has equal affinity for both the electronegative carbonyl site and the "softer" and more diffuse π-cloud on EC.

Conflicts of interest

The authors declare that there are no competing interests or conflicts of interest.

Data availability

The data supporting this article have been included as part of the SI. The Supplementary Information includes additional spectra, atomic co-ordinates corresponding to optimized geometries, and theoretical predictions at the ωB97XD/6-311++G(d,p) level of theory. See DOI: **https://doi.org/10.1039/d5cp02031j**

References

1 A. Chand, D. K. Sahoo, A. Rana, S. Jena and H. S. Biswal, *Acc. Chem. Res.*, 2020, **53**, 1580–1592.
2 V. Kojasoy and D. J. Tantillo, *Org. Biomol. Chem.*, 2023, **21**, 11–23.
3 S. Scheiner, *CrystEngComm*, 2021, **23**, 6821–6837.
4 A. J. Tursi and E. R. Nixon, *J. Chem. Phys.*, 1970, **53**, 518–521.
5 H. S. Biswal, S. Bhattacharyya, A. Bhattacherjee and S. Wategaonkar, *Int. Rev. Phys. Chem.*, 2015, **34**, 99–160.
6 A. Bhattacherjee, Y. Matsuda, A. Fujii and S. Wategaonkar, *ChemPhysChem*, 2013, **14**, 905–914.
7 A. Bhattacherjee, Y. Matsuda, A. Fujii and S. Wategaonkar, *J. Phys. Chem. A*, 2015, **119**, 1117–1126.
8 E. Arunan, T. Emilsson, H. S. Gutowsky, G. T. Fraser, G. de Oliveira and C. E. Dykstra, *J. Chem. Phys.*, 2002, **117**, 9766–9776.
9 D. Wang, P. Chopra, S. Wategaonkar and A. Fujii, *J. Phys. Chem. A*, 2019, **123**, 7255–7260.
10 H. S. Biswal and S. Wategaonkar, *J. Phys. Chem. A*, 2009, **113**, 12774–12782.
11 J. G. David and H. E. Hallam, *Spectrochim. Acta*, 1965, **21**, 841–850.
12 M. Saggu, N. M. Levinson and S. G. Boxer, *J. Am. Chem. Soc.*, 2012, **134**, 18986–18997.
13 K. Grzechnik, K. Rutkowski and Z. Mielke, *J. Mol. Struct.*, 2012, **1009**, 96–102.
14 I. A. Lobo, P. A. Robertson, L. Villani, D. J. D. Wilson and E. G. Robertson, *J. Phys. Chem. A*, 2018, **122**, 7171–7180.
15 F. Torres-Hernandez, P. Pinillos, W. Li, R. T. Saragi, A. Camiruaga, M. Juanes, I. Usabiaga, A. Lesarri and J. A. Fernandez, *J. Phys. Chem. Lett.*, 2024, **15**, 5674–5680.
16 R. T. Saragi, M. Juanes, C. Pérez, P. Pinacho, D. S. Tikhonov, W. Caminati, M. Schnell and A. Lesarri, *J. Phys. Chem. Lett.*, 2021, **12**, 1367–1373.
17 B. Zhang, C. Lv, W. Li, Z. Cui, D. Chen, F. Cao, F. Miao and L. Zhou, *Chem. Pharm. Bull.*, 2015, **63**, 255–262.
18 M. N. Clifford, *J. Sci. Food Agric.*, 2000, **80**, 1033–1043.
19 F. Adebesin, J. R. Widhalm, B. Boachon, F. Lefèvre, B. Pierman, J. H. Lynch, I. Alam, B. Junqueira, R. Benke, S. Ray, J. A. Porter, M. Yanagisawa, H. Y. Wetzstein, J. A. Morgan, M. Boutry, R. C. Schuurink and N. Dudareva, *Science*, 2017, **356**, 1386–1388.
20 S. Bhattacharyya, A. Bhattacherjee, P. R. Shirhatti and S. Wategaonkar, *J. Phys. Chem. A*, 2013, **117**, 8238–8250.
21 A. Bhattacherjee, Y. Matsuda, A. Fujii and S. Wategaonkar, *J. Phys. Chem. A*, 2015, **119**, 1117–1126.
22 M. J. Frisch, G. W. Trucks, H. B. Schlegel, G. E. Scuseria, M. A. Robb, J. R. Cheeseman, G. Scalmani, V. Barone, B. Mennucci, G. A. Petersson, H. Nakatsuji, M. Caricato, X. Li, H. P. Hratchian, A. F. Izmaylov, J. Bloino, G. Zheng, J. L. Sonnenberg, M. Hada, M. Ehara, K. Toyota, R. Fukuda, J. Hasegawa, M. Ishida, T. Nakajima, Y. Honda, O. Kitao, H. Nakai, T. Vreven, J. A. Montgomery, Jr., J. E. Peralta, F. Ogliaro, M. Bearpark, J. J. Heyd, E. Brothers, K. N. Kudin, V. N. Staroverov, R. Kobayashi, J. Normand, K. Raghavachari, A. Rendell, J. C. Burant, S. S. Iyengar, J. Tomasi, M. Cossi, N. Rega, J. M. Millam, M. Klene, J. E. Knox, J. B. Cross, V. Bakken, C. Adamo, J. Jaramillo, R. Gomperts, R. E. Stratmann, O. Yazyev, A. J. Austin, R. Cammi, C. Pomelli, J. W. Ochterski, R. L. Martin, K. Morokuma, V. G. Zakrzewski, G. A. Voth, P. Salvador, J. J. Dannenberg, S. Dapprich, A. D. Daniels, Ö. Farkas, J. B. Foresman, J. V. Ortiz, J. Cioslowski and D. J. Fox, *Gaussian 09, Revision D.01*, Gaussian, Inc., Wallingford CT, 2009.
23 Y. Zhao and D. G. Truhlar, *Acc. Chem. Res.*, 2008, **41**, 157–167.
24 A. R. Neves, P. A. Fernandes and M. J. Ramos, *J. Chem. Theory Comput.*, 2011, **7**, 2059–2067.
25 J.-D. Chai and M. Head-Gordon, *Phys. Chem. Chem. Phys.*, 2008, **10**, 6615–6620.
26 M. Cossi, N. Rega, G. Scalmani and V. Barone, *J. Comput. Chem.*, 2003, **24**, 669–681.
27 M. H. Jamróz, *Spectrochim. Acta, Part A*, 2013, **114**, 220–230.
28 M. W. Schmidt, K. K. Baldridge, J. A. Boatz, S. T. Elbert, M. S. Gordon, J. H. Jensen, S. Koseki, N. Matsunaga, K. A. Nguyen, S. J. Su, T. L. Windus, M. Dupuis and J. A. Montgomery, General Atomic and Molecular Electronic Structure System, *J. Comput. Chem.*, 1993, **14**, 1347–1363.
29 R. F. W. Bader, *Atoms in Molecules-A Quantum Theory*, Oxford University Press, Oxford, (1990).
30 U. Koch and P. L. A. Popelier, *J. Phys. Chem.*, 1995, **99**, 9747–9754.
31 P. Banerjee and T. Chakraborty, *Int. Rev. Phys. Chem.*, 2018, **37**, 83–123.
32 T. S. Zwier, *Annu. Rev. Phys. Chem.*, 1996, **47**, 205–241.
33 J. Zheng, K. Kwak, J. Asbury, X. Chen, I. R. Piletic and M. D. Fayer, *Science*, 2005, **309**, 1338–1343.

